



Nanoscale oxygen defect gradients in UO_{2+x} surfaces

Steven R. Spurgeon^{a,1}, Michel Sassi^b, Colin Ophus^c, Joanne E. Stubbs^d, Eugene S. Ilton^b, and Edgar C. Buck^a

^aEnergy and Environment Directorate, Pacific Northwest National Laboratory, Richland, WA 99352; ^bPhysical and Computational Sciences Directorate, Pacific Northwest National Laboratory, Richland, WA 99352; ^cNational Center for Electron Microscopy, Molecular Foundry, Lawrence Berkeley National Laboratory, Berkeley, CA 94720; and ^dCenter for Advanced Radiation Sources, The University of Chicago, Chicago, IL 60439

Edited by David L. Clark, Los Alamos National Laboratory, Los Alamos, NM, and accepted by Editorial Board Member Richard Eisenberg July 15, 2019 (received for review March 25, 2019)

Oxygen defects govern the behavior of a range of materials spanning catalysis, quantum computing, and nuclear energy. Understanding and controlling these defects is particularly important for the safe use, storage, and disposal of actinide oxides in the nuclear fuel cycle, since their oxidation state influences fuel lifetimes, stability, and the contamination of groundwater. However, poorly understood nanoscale fluctuations in these systems can lead to significant deviations from bulk oxidation behavior. Here we describe the use of aberration-corrected scanning transmission electron microscopy and electron energy loss spectroscopy to resolve changes in the local oxygen defect environment in UO_{2+x} surfaces. We observe large image contrast and spectral changes that reflect the presence of sizable gradients in interstitial oxygen content at the nanoscale, which we quantify through first-principles calculations and image simulations. These findings reveal an unprecedented level of excess oxygen incorporated in a complex near-surface spatial distribution, offering additional insight into defect formation pathways and kinetics during UO_2 surface oxidation.

actinide oxides | uraninite | surface oxidation | scanning transmission electron microscopy | electron energy loss spectroscopy

The engineering of oxygen defects is a central focus of modern materials science. These defects influence the electronic, magnetic, optical, and radiation-response properties of materials in ways that are difficult to control and predict a priori (1–3). In particular, the safe use and disposal of oxide-based nuclear fuels depend on comprehensive models for oxidative processes and defect formation, which can guide operation, long-term waste storage, and accident cleanup efforts (4). Because of their strategic importance and potential environmental impact (5), the oxidative behavior of the actinides has attracted considerable attention. These $5f$ elements exist in multiple valence states in oxides, leading to electronic properties and phase transitions that are a sensitive function of oxygen defects.

Among the actinides, hyperstoichiometric UO_{2+x} has been examined for over half a century because of its central role in fuel production, as well as its many interesting properties (6–10). The system can adopt at least 14 known fluorite-derivative crystal structures, with oxidation states spanning $\text{U}^{4+} \rightarrow \text{U}^{6+}$, the latter of which is aqueous soluble and a risk driver for environmental transport (7, 8, 11). The complex chemical landscape of this system has motivated longstanding questions about the nature of these phase transitions and the incorporation of excess oxygen. Prior work indicated that a stoichiometry of $\text{UO}_{2.25}$ is readily attainable while preserving the nominal fluorite structure (12). However, several studies have identified metastable higher oxides possessing a fluorite-like structure, including U_3O_7 (13, 14) and U_3O_8 (15). The former studies found that the U sublattice is very similar between UO_2 and higher oxides up to U_3O_8 and that the main differences arise in the O anion sublattice. The latter study showed that it is possible to stabilize fluorite-like U_3O_8 at high temperature and pressure, which is retained upon quenching to ambient conditions. This experimental work is further supported by theory calculations (16, 17), which indicate that stoichiometries up to $\text{UO}_{2.5}$ should be pos-

sible within the fluorite-like structure. Together, these studies suggest that the primary impact of excess oxygen will be on the type and distribution of O anion defects, rather than a sizable distortion of the U cation sublattice. It is clear that nanoscale deviations from predicted bulk behavior, as well as nonequilibrium synthesis pathways, can greatly affect the oxidation process, calling for a more precise local understanding between phase transitions and oxygen defect formation.

While a large body of experimental and computational work has attempted to elucidate defect formation kinetics and oxidation pathways of UO_2 , the task is hindered by a lack of well-controlled model systems and the difficulty of simulating strongly correlated $5f$ electrons (6, 8, 18). Most studies have relied on volume-averaged techniques, such as X-ray absorption near-edge structure (XANES), extended X-ray absorption fine structure (EXAFS), and X-ray photoelectron spectroscopy (XPS), applied to polycrystalline samples (19–22). When these measurements are interpreted through first-principles calculations, they can yield powerful insight into electronic structure, local coordination environment, and valence (21, 23, 24). In addition, X-ray crystal truncation rod (CTR) analysis has been shown to resolve surface distortions and subsurface oxygen interstitial profiles in single-crystal UO_2 , albeit over a millimeter-sized region of a sample (25, 26). Through fitting the CTR data and computational modeling, the authors inferred the development of oscillatory interstitial O profiles under the (001)- and (111)-oriented surfaces of UO_2 . However, the large atomic number contrast between U and O, as well as the large lateral area

Significance

Our study has far-reaching implications for the safe use of nuclear materials around the world. The strong oxidative tendency of the actinides drives contamination of groundwater near waste storage sites. A key finding of our study is that excess oxygen from the environment can be incorporated at far greater levels than previously thought, while still preserving the nominal cubic crystal structure of the widely used nuclear fuel UO_2 . This insight, enabled by atomic-resolution spectroscopy and theory calculations, will allow us to develop better, more reliable models for nuclear waste storage and disposal.

Author contributions: S.R.S., M.S., C.O., J.E.S., E.S.I., and E.C.B. designed research; S.R.S., M.S., and C.O. performed research; C.O. contributed new reagents/analytic tools; S.R.S., M.S., C.O., J.E.S., E.S.I., and E.C.B. analyzed data; and S.R.S., M.S., C.O., J.E.S., E.S.I., and E.C.B. wrote the paper.

The authors declare no conflict of interest.

This article is a PNAS Direct Submission. D.L.C. is a guest editor invited by the Editorial Board.

This open access article is distributed under [Creative Commons Attribution-NonCommercial-NoDerivatives License 4.0 \(CC BY-NC-ND\)](#).

Data deposition: Data from this study have been deposited in Figshare, <https://figshare.com/articles/Spurgeon.UO2.PNAS.Data.Archive/9108503/1>.

¹To whom correspondence may be addressed. Email: steven.spurgeon@pnnl.gov.

This article contains supporting information online at www.pnas.org/lookup/suppl/doi:10.1073/pnas.1905056116/-DCSupplemental.

Published online August 9, 2019.

over which the measurements were averaged, precluded the direct observation of interstitial geometries and localized atomic environments.

A major strength of scanning transmission electron microscopy and electron energy loss spectroscopy (STEM-EELS) approaches is that they provide high-resolution, simultaneous information about local structure, chemistry, and defects. Past studies have shown that STEM-EELS is capable of detecting minor changes in oxidation state and composition and that it compares favorably to X-ray results on similar uranium compounds (27–30). Within the dipole approximation, these results can also be modeled using first-principles methods, offering a means to quantify defect configurations and density (27, 31). However, early STEM-EELS work on the actinides was performed using slower, lower-resolution spectrometers (32–37) and few studies (38, 39) have leveraged the advanced instrumentation or the supporting first-principles computing power developed in recent years. Modern aberration-corrected microscopes, equipped with bright, subangstrom electron probes and high-speed EELS spectrometers, now permit true atomic-scale spectroscopy with exceptional energy resolution (40). Studies of complex oxides have shown that it is possible to examine image contrast (41) and spectral changes (42, 43) associated with oxygen defects at interfaces and around local inhomogeneities that lead to significant deviations from bulk properties, but are difficult to access via other means. These as-yet untapped techniques may inform atomistic mechanisms for uranium oxidation.

Here we compare the behavior of model oxidized (001)- and unoxidized (111)-oriented single-crystal UO_2 surfaces using a combination of aberration-corrected STEM imaging and spectroscopy supported by first-principles theory and image simulations. Data pertaining to this study have been deposited in Figshare (“Spurgeon UO2 PNAS Data Archive,” https://figshare.com/articles/Spurgeon_UO2_PNAS_Data_Archive/9108503/1) (44). Previous X-ray CTR results (25, 26) have indicated that the former surface exhibits a 2-layer periodicity in surface-normal lattice contraction, which was indirectly related to the insertion of O interstitials. We present an atomically resolved STEM-EELS mapping of the U $M_{4,5}$ edge, as well as a detailed examination of the O K edge fine structure in the vicinity of the crystal surface. This combination of techniques provides unique insight into the basis for image contrast and the emergence of key spectral features that result from the

incorporation of excess oxygen in the near-surface region. We quantify the local interstitial content at the nanoscale, finding a large amount of excess oxygen distributed across a gradient near the sample surface; however, we see no evidence for a large-scale phase transition from the fluorite structure even at stoichiometries approaching $\text{UO}_{2.67}$. Finally, we identify how these gradients impact the prior understanding of UO_2 oxidation and discuss how they might also inform the analysis of other actinides. Our results illustrate how direct, real-space imaging approaches can inform our understanding of oxygen defect formation in actinide oxides.

As described in *SI Appendix*, we prepared 2 model UO_2 single-crystal surfaces: An unoxidized (111)-oriented control sample stored in an inert gas environment and a heavily oxidized (001) sample exposed to pure O_2 for 21 d, followed by storage in ambient conditions for several months. The former has been predicted to be the most stable UO_2 surface when dry (25). We examined the cross-sectional structure of the near-surface region for each sample at atomic resolution, as shown in Fig. 1. These images were acquired in the incoherent STEM high-angle annular dark field (STEM-HAADF) imaging mode, whose contrast is approximately proportional to atomic number $Z^{\sim 1.7}$; this mode is insensitive to the thickness-dependent contrast reversals that complicate the interpretation of typical high-resolution transmission electron micrographs (45). Both samples, shown in Fig. 1 *A* and *B*, exhibited a single-crystalline structure free of extended defects or impurities and we confirmed a nominal cubic fluorite structure throughout, as described in *SI Appendix*. However, there is a striking difference in the contrast of the (001) crystal surface, which exhibited an ~ 15 -nm band of increased intensity. This band was present in all of the oxidized samples prepared and was not the result of carbon contamination or thickness variation, as confirmed by imaging and low-loss EELS shown in *SI Appendix*, Figs. S1 and S2. We also performed geometric phase analysis (GPA) to assess possible strain variations at the nanoscale, as shown in *SI Appendix*, Fig. S3. These results suggest that no large-scale phase transformation has occurred at the sample surface and that lattice bending is not responsible for the contrast band.

Interestingly, a study of CeO_2 nanoparticles (41) found that changes in ionic radius upon oxidation from $\text{Ce}^{3+} \rightarrow \text{Ce}^{4+}$ can impart static lattice displacements to the crystal; this, in turn, can influence electron channeling and induce sizable changes in

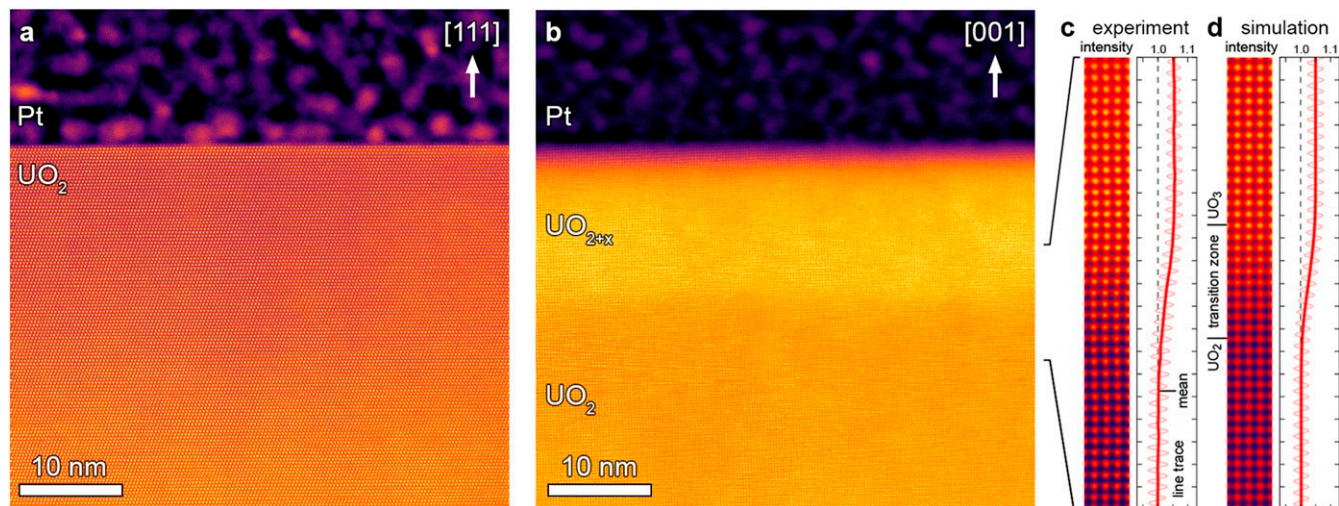


Fig. 1. Imaging and simulation of the UO_2 sample surfaces. (*A* and *B*) Colorized cross-sectional STEM-HAADF images of the unoxidized (111)-oriented (*A*) and oxidized (001)-oriented (*B*) UO_2 sample surfaces, respectively. These images are taken along the [110] and [100] zone axes, respectively. (*C* and *D*) Experimental (*C*) and simulated (*D*) mean unit cells, and corresponding line traces, for the (001) sample.

comparable to the highest U_3O_8 stoichiometry obtained during high-pressure synthesis (15), and in excess of prior reports on the formation of U_3O_7 (13, 14), representing a significant departure from bulk behavior. Considering the nonequilibrium nature of the oxidative process, we emphasize the competition of the bulk and surface states of the crystal. Analogous to substrate-induced “clamping” in multiferroic oxide heterostructures (52), it is likely that structural distortions of the surface are constrained by the underlying bulk, limiting associated phase transitions. The competition between transport of oxygen into the bulk and reduction of the surface may also give rise to the observed gradient in oxygen interstitial content. These nanoscale insights can help refine our understanding of oxygen transport and defect formation kinetics in this system. More broadly, our study shows how a combination of STEM, EELS, and first-principles calculations may be used to fingerprint the local chemical environment of actinide surfaces. Substantial excess oxygen manifests in image contrast changes that are accompanied by unique spectral signatures in the O K edge fine structure. Our simulations are able to disentangle key contributors to these signatures, identifying likely oxygen configurations that can be examined in other related systems. Using this approach, it is now possible to examine defect

generation at surfaces and interfaces, such as grain boundaries in altered spent nuclear fuel pellets or other actinide oxide waste forms, paving the way for more comprehensive atomistic models for oxidative behavior.

Additional Information

SI Appendix details the methods used, imaging, thickness measurements, strain analysis, multislice simulation, and first-principles calculations. Correspondence and requests for materials should be addressed to S.R.S.

ACKNOWLEDGMENTS. S.R.S. thanks Drs. Kevin Rosso, Demie Kepaptsoglou, and Lewys Jones for helpful discussions. Pacific Northwest National Laboratory (PNNL) is a multiprogram national laboratory operated for the Department of Energy (DOE) by Battelle. This work was supported by the Nuclear Process Science Initiative at PNNL. A portion of the microscopy was performed in the Radiological Microscopy Suite, located in the Radiochemical Processing Laboratory at PNNL. Work at the Molecular Foundry was supported by the Office of Science, Office of Basic Energy Sciences, of the US DOE under Contract DE-AC02-05CH11231. C.O. acknowledges support from the DOE Early Career Research Program. J.E.S. is supported by the National Science Foundation-Earth Sciences (EAR-1634415) and DOE-GeoSciences (DE-FG02-94ER14466 and DE-SC0019108). We thank R. Caciuffo (Institute for Transuranium Elements) and M. Paffett (Los Alamos National Laboratory) for providing the UO_2 crystals.

- H. L. Tuller, S. R. Bishop, Point defects in oxides: Tailoring materials through defect engineering. *Annu. Rev. Mater. Res.* **41**, 369–398 (2011).
- M. Verónica Ganduglia-Pirovano, A. Hofmann, J. Sauer, Oxygen vacancies in transition metal and rare earth oxides: Current state of understanding and remaining challenges. *Surf. Sci. Rep.* **62**, 219–270 (2007).
- K. E. Sickafus *et al.*, Radiation tolerance of complex oxides. *Science* **289**, 748–751 (2000).
- P. C. Burns, R. C. Ewing, A. Navrotsky, Nuclear fuel in a reactor accident. *Science* **335**, 1184–1188 (2012).
- R. M. Coyte *et al.*, Large-scale uranium contamination of groundwater resources in India. *Environ. Sci. Technol.* **5**, 341–347 (2018).
- M. W. D. Cooper, S. T. Murphy, D. A. Andersson, The defect chemistry of $UO_{2\pm x}$ from atomistic simulations. *J. Nucl. Mater.* **504**, 251–260 (2018).
- D. W. Shoesmith, Fuel corrosion processes under waste disposal conditions. *J. Nucl. Mater.* **282**, 1–31 (2000).
- R. J. McEachern, P. Taylor, A review of the oxidation of uranium dioxide at temperatures below 400 °C. *J. Nucl. Mater.* **254**, 87–121 (1998).
- E. S. Fisher, The first 30 years of research on the physical properties of α -U. *J. Alloys Compd.* **213–214**, 254–261 (1994).
- B. Wasserstein, Ages of uraninites by a new method. *Nature* **174**, 1004–1005 (1954).
- K. O. Kvashnina, S. M. Butorin, P. Martin, P. Glatzel, Chemical state of complex uranium oxides. *Phys. Rev. Lett.* **111**, 253002 (2013).
- B. T. M. Willis, The defect structure of hyper-stoichiometric uranium dioxide. *Acta Crystallogr. Sect. A* **34**, 88–90 (1978).
- L. Desgranges, G. Baldinozzi, G. Rousseau, J.-C. Niepce, G. Calvarin, Neutron diffraction study of the in situ oxidation of UO_2 . *Inorg. Chem.* **48**, 7585–7592 (2009).
- F. Garrido, R. M. Ibberson, L. Nowicki, B. T. M. Willis, Cuboctahedral oxygen clusters in U_3O_7 . *J. Nucl. Mater.* **322**, 87–89 (2003).
- F. X. Zhang *et al.*, High-pressure U_3O_8 with the fluorite-type structure. *J. Solid State Chem.* **213**, 110–115 (2014).
- D. A. Andersson, G. Baldinozzi, L. Desgranges, D. R. Conradson, S. D. Conradson, Density functional theory calculations of UO_{2+x} , U_4O_9-y , U_3O_7 , and U_3O_8 . *Inorg. Chem.* **52**, 2769–2778 (2013).
- M. Molinari, N. A. Brincat, G. C. Allen, S. C. Parker, Structure and properties of some layered U_2O_5 phases: A density functional theory study. *Inorg. Chem.* **56**, 4468–4473 (2017).
- T. Vitova *et al.*, The role of the 5f valence orbitals of early actinides in chemical bonding. *Nat. Commun.* **8**, 1–9 (2017).
- J. G. Tobin *et al.*, Covalency in oxidized uranium. *Phys. Rev. B* **92**, 045130 (2015).
- D. L. Clark, *Chemical bonding in molecules with valence 5f-electrons*. <https://www.osti.gov/servlets/purl/1119596>. Accessed 1 June 2019.
- S.-W. Yu *et al.*, f-f origin of the insulating state in uranium dioxide: X-ray absorption experiments and first-principles calculations. *Phys. Rev. B* **83**, 165102 (2011).
- E. S. Ilton, P. S. Bagus, XPS determination of uranium oxidation states. *Surf. Interface Anal.* **43**, 1549–1560 (2011).
- Z. Y. Wu *et al.*, X-ray absorption at the oxygen K edge in cubic f oxides examined using a full multiple-scattering approach. *J. Phys. Condens. Matter* **11**, 7185–7194 (1999).
- F. Jollet *et al.*, The electronic structure of uranium dioxide: An oxygen K-edge x-ray absorption study. *J. Phys. Condens. Matter* **9**, 9393–9401 (1997).
- J. E. Stubbs *et al.*, Oxidative corrosion of the $UO_2(001)$ surface by nonclassical diffusion. *Langmuir* **33**, 13189–13196 (2017).
- J. E. Stubbs *et al.*, UO_2 oxidative corrosion by nonclassical diffusion. *Phys. Rev. Lett.* **114**, 246103 (2015).
- A. K. Jiang *et al.*, Determination of interstitial oxygen atom position in $U_2N_3+xO_y$ by near edge structure study. *J. Nucl. Mater.* **504**, 215–220 (2018).
- J. G. Tobin, D. K. Shuh, Electron spectroscopy of the oxidation and aging of U and Pu. *J. Electron Spectros. Relat. Phenom.* **205**, 83–91 (2015).
- R. Caciuffo, E. C. Buck, D. L. Clark, G. Van Der Laan. Spectroscopic characterization of actinide materials. *MRS Bull.* **35**, 889–895 (2010).
- K. T. Moore *et al.*, Electron-energy-loss spectroscopy and X-ray absorption spectroscopy as complementary probes for complex f-electron metals: Cerium and plutonium. *Philos. Mag.* **84**, 1039–1056 (2004).
- J. A. Aguiar, Q. M. Ramasse, M. Asta, N. D. Browning, Investigating the electronic structure of fluorite-structured oxide compounds: Comparison of experimental EELS with first principles calculations. *J. Phys. Condens. Matter* **24**, 295503 (2012).
- S. Utsunomiya, M. Kogawa, E. Kamiishi, R. C. Ewing, “Scanning transmission electron microscopy and related techniques for research on actinide and radionuclide nanomaterials” in *Actinide Nanoparticle Research* (Springer Berlin Heidelberg, Berlin, Heidelberg, Germany, 2011), pp. 33–62.
- E. C. Buck, M. Douglas, R. S. Wittman, Verifying the presence of low levels of neptunium in a uranium matrix with electron energy-loss spectroscopy. *Micron* **41**, 65–70 (2010).
- M. Colella, G. R. Lumpkin, Z. Zhang, E. C. Buck, K. L. Smith, Determination of the uranium valence state in the brannerite structure using EELS, XPS, and EDX. *Phys. Chem. Miner.* **32**, 52–64 (2005).
- S. L. Dudarev *et al.*, Understanding STM images and EELS spectra of oxides with strongly correlated electrons: A comparison of nickel and uranium oxides. *Micron* **31**, 363–372 (2000).
- S. B. Rice, H. H. Bales, J. R. Roth, A. L. Whiteside, Empirical identification of uranium oxides and fluorides using electron energy-loss spectroscopy in the transmission electron microscope. *Microsc. Microanal.* **5**, 437–444 (1999).
- H. Xu, Y. Wang, Electron energy-loss spectroscopy (EELS) study of oxidation states of Ce and U in pyrochlore and uraninite – natural analogues for Pu- and U-bearing waste forms. *J. Nucl. Mater.* **265**, 117–123 (1999).
- A. Ochiai *et al.*, Uranium dioxides and debris fragments released to the environment with cesium-rich microparticles from the Fukushima Daiichi nuclear power plant. *Environ. Sci. Technol.* **52**, 2586–2594 (2018).
- C. Degueldre, R. Schaeublin, J. Krbanjevic, E. Minikus, Electron energy loss spectroscopy investigation through a nano ablated uranium dioxide sample. *Talanta* **106**, 408–413 (2013).
- O. L. Krivanek *et al.*, An electron microscope for the aberration-corrected era. *Ultramicroscopy* **108**, 179–195 (2008).
- A. C. Johnston-Peck *et al.*, Oxidation-state sensitive imaging of cerium dioxide by atomic-resolution low-angle annular dark field scanning transmission electron microscopy. *Ultramicroscopy* **162**, 52–60 (2016).
- J. A. Mundy, Q. Mao, C. M. Brooks, D. G. Schlom, D. A. Muller, Atomic-resolution chemical imaging of oxygen local bonding environments by electron energy loss spectroscopy. *Appl. Phys. Lett.* **101**, 042907 (2012).
- M. Varela *et al.*, Atomic-resolution imaging of oxidation states in manganites. *Phys. Rev. B* **79**, 085117 (2009).
- S. Spurgeon *et al.*, Data from “Spurgeon UO_2 PNAS Data Archive.” Figshare. 10.6084/m9.figshare.9108503.v1. Deposited 25 July 2019.
- D. B. Williams, C. B. Carter, *Transmission Electron Microscopy* (Springer, 2009).
- R. D. Shannon, Revised effective ionic radii and systematic studies of interatomic distances in halides and chalcogenides. *Acta Crystallogr. Sect. A* **32**, 751–767 (1976).

47. C. L. Tracy *et al.*, Redox response of actinide materials to highly ionizing radiation. *Nat. Commun.* **6**, 1–9 (2015).
48. L.-M. Peng, Electron atomic scattering factors and scattering potentials of crystals. *Micron* **30**, 625–648 (1999).
49. J. A. Fortner, E. C. Buck, A. J. G. Ellison, J. K. Bates, EELS analysis of redox in glasses for plutonium immobilization. *Ultramicroscopy* **67**, 77–81 (1997).
50. J. A. Aguiar *et al.*, Electronic structure of oxide fuels from experiment and first principles calculations., *J. Phys. Conf. Ser.* **241**, 012062 (2010).
51. O. Bunău, Y. Joly, Self-consistent aspects of x-ray absorption calculations. *J. Phys. Condens. Matter* **21**, 345501 (2009).
52. I. Bichurin, M. Petrov, G. Srinivasan, Theory of low-frequency magnetoelectric coupling in magnetostrictive-piezoelectric bilayers. *Phys. Rev. B Condens. Matter Mater. Phys.* **68**, 1–13 (2003).